Electron Emission Projection Imager

Stanislav S. Baturin* and Sergey V. Baryshev†
Euclid TechLabs, 365 Remington Blvd., Bolingbrook, IL 60440, USA

A new projection type imaging system is presented. The system can directly image the field emission site distribution on a cathode surface by making use of anode screens in the standard parallel plate configuration. The lateral spatial resolution of the imager is on the order of 1 μm. The imaging sensitivity to the field emission current can be better than the current sensitivity of a typical electrometer, i.e. less than 1 nA.

arXiv:1611.05929v2 [physics.ins-det] 25 Dec 2016

Introduction

In situ real-time or time-resolved imaging at micro- and nano-scales has provided a great deal of understanding of various processes that take place in materials. Many contemporary imaging concepts are intrinsically based on raster scanning. This means that the pointed focused/sharp probe, be it an electron or ion probe, or a mechanical cantilever, scans across a given area to resolve and plot an image of a static or dynamic pattern. Such images consist of pixels or voxels containing locally collected information. Examples are SEM, STEM, STM, AFM, imaging TOF SIMS, and others.

A second approach is much older and comes from photography. This is the projection method and it is entirely different from raster scanning. In this approach, a surface of interest under electromagnetic irradiation or electron bombardment is imaged at a certain distance beyond the interaction location giving rise to a significant magnification. Examples are electron diffraction in TEM and LEED, and X-ray topography. The most remarkable examples here would be the field emission microscope and field ion microscope invented by Erwin Mueller, in which electron or ion imaging of a sharp tip placed in a high electric field becomes possible with nanometer or atomic resolution without complex motorized systems, data acquisition, and post-processing methods.

In the realm of finding inexpensive, reliable and adaptive field emission sources, beyond Spindt cathodes, to drive various devices and systems, many novel advanced materials have been studied. This research field remains extremely active and is of significant interest to this very day. Field emission sources often yield laterally non-uniform emission. This is because field emission is a non-linear process and therefore surface termination and geometrical features contribute significantly to the surface barrier formation and its lateral uniformity. Thus, in practice a packaged field emission source will always have strong and weak emission points.

To the best of our knowledge, systems to observe the lateral uniformity of field emission arrays are always raster-scanning tools that move a micron scale anode tip across a field emitter surface [1–3]. In this paper, we present an electron emission projection imager system that captures lateral emitter distribution of the entire surface instantaneously.

General description of the imager. Imaging and measurement examples

The conceptual diagram of the imaging system and its actual appearance are shown in Fig.1. The imager has three anodes (1) an optically polished (1 inch dia. and 100 μm thick) disk made of yttrium aluminum garnet doped with cerium (YAG:Ce) which is coated with a Mo film of about 7-8 nm in thickness; (2) a transparent and conductive tin-doped indium oxide (ITO) film of 175 nm deposited onto a boro-aluminosilicate glass (BASG) substrate of 700 μm in thickness; (3) a polished (1 inch dia. and 100 μm thick) disk made of stainless steel (SS).

The Mo/YAG:Ce and ITO/BASG anodes are imaging screens and the SS anode is to measure long-term temporal current stability. Mo/YAG:Ce and ITO/BASG are semitransparent in the visible range. Fig.2a illustrates detailed UV-vis. spectra and Fig.2b demonstrates transparency when anode screens covering color lines are backside illuminated.

Depending on the specific measurement to be performed, the anodes can be interchanged by linearly moving the frame holding all three anodes, by means of an ultrahigh vacuum actuator. The distance between the sample and the anode is set using a micrometer holding the sample. Top and side view cameras outside the vacuum are used to check the parallelism between the cathode and anode, and to measure the gap. A Canon DLSR camera is installed at a viewport behind the anodes to take pictures of electron emission patterns. The sample electrode is at ground and the anode frame is isolated and positively biased. The bias and current readings are enabled by a Keithley 2410 electrometer. The Keithley and the Canon are programmed such that they collect data sets of current-voltage (I-V) curves and images synchronously.

Before going into a detailed description of the imager, we would like to introduce a series of pictures taken on a carbon nanotube (CNT) sample grown by a CVD process. Fig.3a illustrates the appearance of the sample in an optical micrograph, Fig.3b illustrates the morphology as measured using a scanning electron microscope (SEM), Fig.3c illustrates the green (550 nm) light produced by the Mo/YAG:Ce anode screen under ∼1 keV and ∼100 μA electron bombardment, and Fig.3d illustrates clus-

*Current address: Department of Physics, The University of Chicago, 5720 S. Ellis Ave., Chicago, IL, 60637, USA

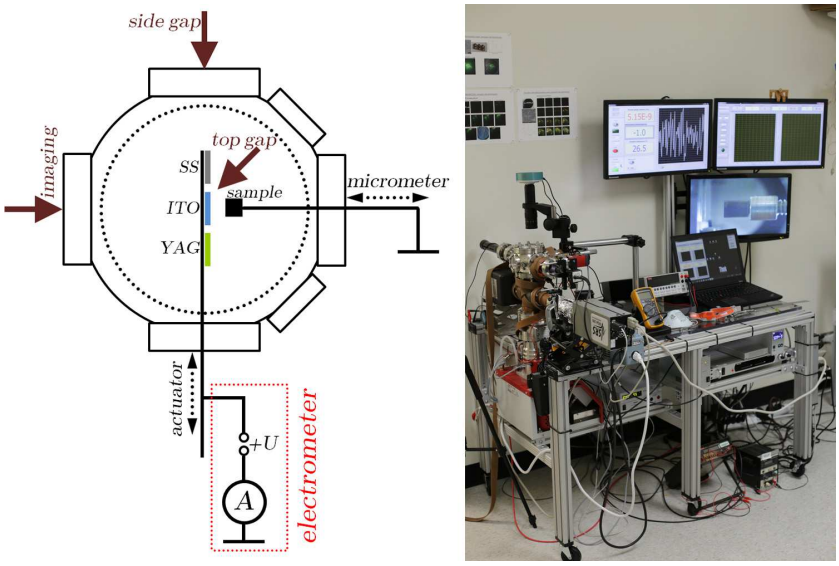

FIG. 1: A schematic of the electron emission imager. Solid arrows represent the 3 cameras: two cameras are used to monitor parallelism between the cathode and anode surfaces upon installation and to measure the interelectrode gap during field emission measurements, and the third camera is used to detect light from either anode screen luminescence or light originating from the cathode surface itself (exampled below), or both

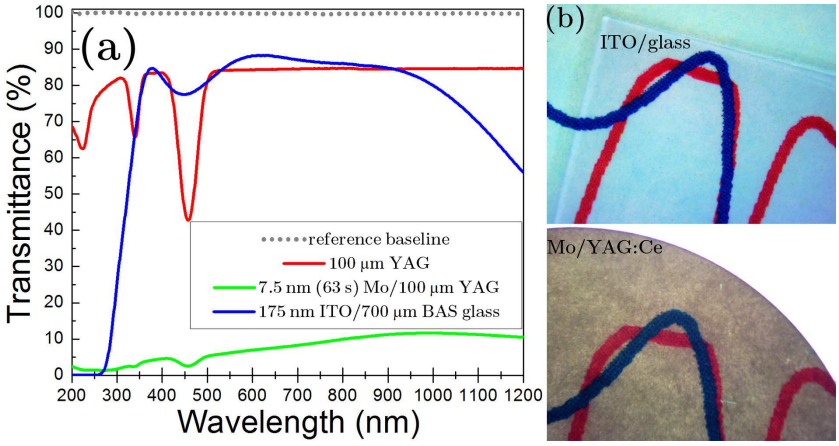

FIG. 2: (a) UV-vis. spectra (spectral dependence of transmittance) for the YAG:Ce (red line), Mo/YAG:Ce (green line) and ITO/BASG (blue line) anode screens. (b) Photographs that demonstrate the semitransparency of the ITO/BASG anode (top) and Mo/YAG:Ce anode (bottom)

ters of intense red light imaged with the ITO/BASG anode screen under similar ∼1 keV and ∼100 μA conditions. The red cores already can be seen in Fig.3c, because the red light intensity is extremely high and the Mo/YAG:Ce screen is semitransparent in the red. The red light thermally produced by CNT due to electric current flow induced heating is a well-known effect which has been documented over the last 15 years [4–8]. Note – the Mo/YAG:Ce and ITO/BASG anode images were taken at different sample installations and different camera presets and therefore the red light patterns do not coincide.

Along with imaging, I-V curves can be collected as demonstrated in Fig.4a. Linear and semi-logarithmic I-V characteristics of the CNT sample are presented. The abscissa is presented in units of electric field after the recorded voltage was divided by the interelectrode gap taken by the top camera (Fig.4b, right). As mentioned, the opaque SS anode is used to measure long-term emission current stability. An example of the results of a long 24 hour run carried out for the CNT sample is shown in Fig.4b.

Spatial resolution of the acquired images is limited by the optical system. For the case shown in Fig.3c, the resolution is 0.8 μm per pixel (the known sample diameter is 4,400 μm and the apparent sample diameter in Fig.3c is 550 pixels). Using another lens we recently were able to achieve a higher optical magnification which resulted in a higher spatial resolution of 0.3 μm per pixel.

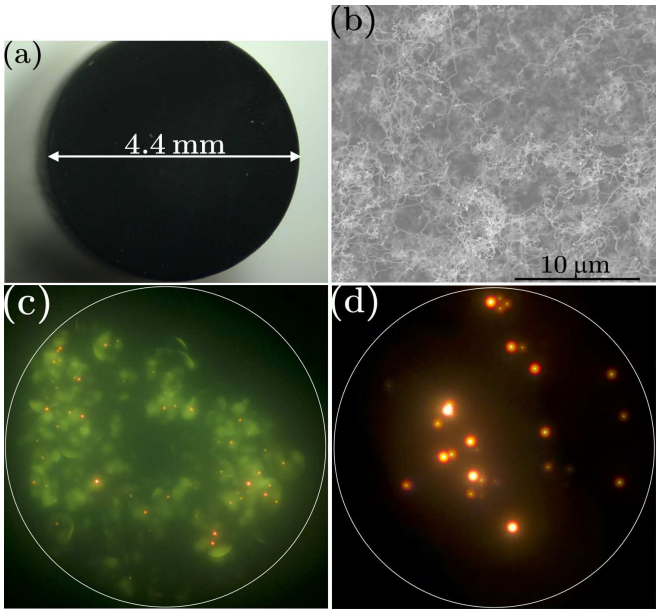

FIG. 3: CNT on stainless steel substrate: (a) an optical microscopy image of the CNT sample; (b) a high magnification SEM image showing the CNT morphology; (c) emission pattern imaged with the Mo/YAG:Ce anode screen; (d) emission pattern imaged with the ITO/BASG anode screen

Detailed description of the apparatus

Imaging screens

ITO/BASG screens were purchased from Delta Technologies. The anode screen is a 1 sq. inch BASG square, 0.7 mm in thickness. An ITO film of approximately 175 nm is deposited on one side of the BASG square. The ITO film resistivity is between 4-10 Ω. The conductive ITO side faces the cathode under measurement conditions.

To establish an electric field between the sample and the isolating YAG:Ce anode and to collect the current, a metal film needs to be deposited. Molybdenum was chosen because it is dense and allows for continuous ultrathin films. In addition, the melting point of Mo is 2,896 K, meaning that Mo coatings can sustain exceptionally high electrical power surface densities $\frac{I \cdot V}{cm^2}$. We specify this because originally Al coatings were used that would melt upon the first run producing bulged anode surfaces at the location where current was collected. Mo is deposited in house by magnetron sputtering on one side of an optical-quality polished YAG:Ce disk. Base pressure in the magnetron system is $<5\times10^{-7}$ Torr. Prior to coating, the YAG:Ce disk is cleaned *in situ* using RF discharge plasma. Without breaking vacuum, immediately after the cleaning, the Mo coating is deposited. Ar is used as a working gas for both cleaning and sputtering at a pressure $\sim10^{-3}$ Torr.

For voltages less than 1.1 kV, provided by the Keithley 2410, the Mo coating has to be ultrathin. A standard deposition time of 60 seconds was found to be optimal for our application. This means the thickness of the resulting Mo film is sufficiently small to let many electrons into the YAG:Ce to produce photons, but thick enough to filter electrons such that they do not penetrate too deeply into the YAG:Ce phosphor – this would lead to charging and discharging effects in the YAG:Ce. For instance, a Mo thickness corresponding to a 60 s deposition time does not comprehend applied voltages over 2 kV. The electron penetration depth becomes such that electrons start accumulating inside the YAG:Ce and do not efficiently drain. This results in luminescence instabilities and may lead to strong discharge events damaging both the YAG:Ce and Mo coatings. The choice of Mo thickness is determined by the application and the voltage range to be applied between the electron emitter under study and the anode.

For specific and quantitative choice of the Mo thickness, the Kanaya-Okayama approach [9] can be used. The following formula relates the electron energy, E [keV], to the electron range, RKO [μm], the maximum possible penetration depth

$$RKO = 27.6 \cdot 10^{-3} \cdot \frac{MM \cdot E^{1.67}}{Z^{0.889} \cdot \rho}, \quad (1)$$

where MM is the molar mass [g/mol], Z is the atomic number, ρ is the mass density [g/cm^3]. The resulting dependence is shown in Fig.5, and provides a precise answer for the maximum thickness of Mo. The example calculation at 1 keV yields RKO=9.3 nm. In practice, one would use not the maximum range but rather so-called practical range which is about 0.7 of RKO [10]. This leads to a specific requirement on the Mo coating – 6.5 nm. At this Mo thickness, about 10% of electrons that were not back scattered, will penetrate into the YAG:Ce and produce photons.

Now we can explain why the deposition time of 60 seconds works best for the 1.1 keV application by converting the deposition time into the actual thickness of the Mo coating. To measure the thickness of the Mo coating, we synthesized three test samples on optically polished Si witness coupons and depth profiled them using secondary ion mass spectrometry (SIMS). One sample was deposited for 60 s (the same time used for YAG:Ce anode fabrication), and two others were deposited for 90 s and 120 s. With SIMS, it is possible to measure the thickness. By definition, sputtering rate (SR) is calculated by dividing the layer thickness d by the time T it took to sputter through it. On the other hand, the SR can be expressed through other experimental and fundamental material parameters: the ion current density j, the sputtering yield (i.e., the number of ejected atoms per incident ion) Y, the elementary charge e, and the atomic density of the target material (units of atoms per volume) N, or alternatively the mass density of the target material ρ and the atomic mass of the target material M. Combining everything together, we can deduce a formula for the thickness of the layer to be determined as

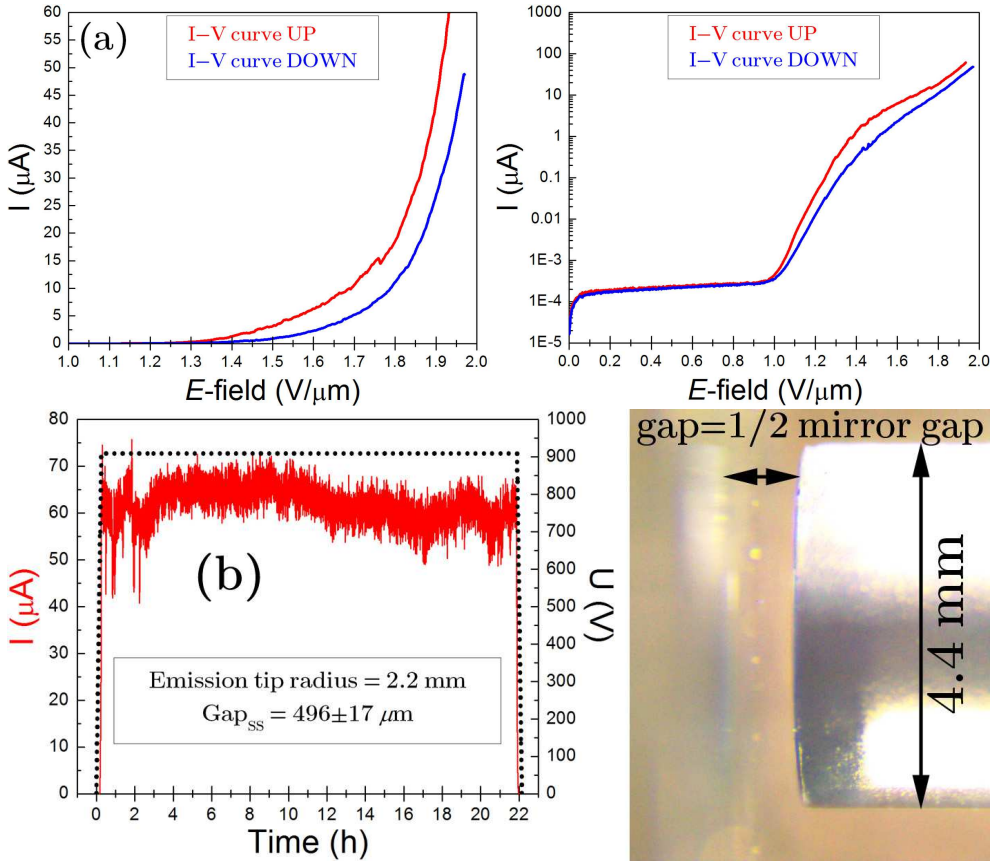

FIG. 4: Electric characterization of the CNT sample: (a) I-V characteristics in linear and semi-log representation and (b) current time stability measurement taken over a 24 hour period. The right panel demonstrates an example of electrode parallelism and the gap between the SS anode and the CNT cathode measured as 496 μm

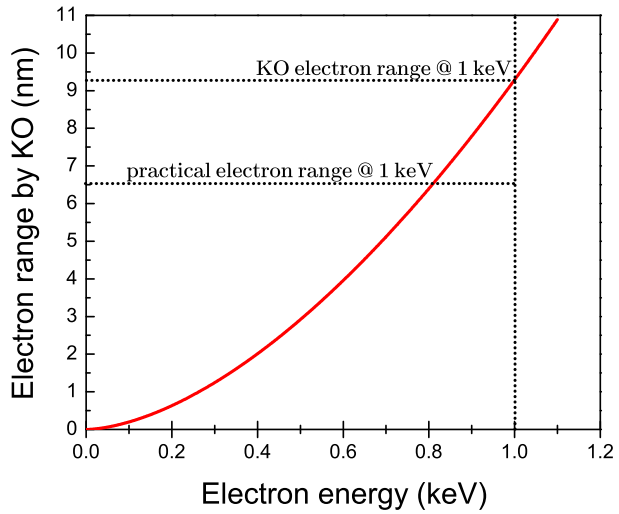

FIG. 5: The dependence of the electron range on the energy, calculated for Mo using the KO formula, Eq.(1)

$$\begin{cases} SR = \frac{d}{T} \\ SR = \frac{j \cdot Y}{e \cdot N} \end{cases} \Longrightarrow d = T \cdot \frac{j \cdot Y \cdot M}{e \cdot \rho} \quad . \quad (2)$$
$$N = \frac{\rho}{M}$$

The test samples were depth profiled using a time-of-flight SIMS instrument in the traditional single beam mode [11]. The 60° oblique 5 kV Ar^+ ion beam was focused to a spot of 30 μm in diameter at a current of 80±8 nA as measured by *in situ* Faraday cup. When depth profiling, the beam was raster scanned over an area of 675×675 μm^2, yielding an ion current density $j = 17.6 \pm 1.8$ $\mu A/cm^2$. Both the single ion beam spot and the raster sizes were measured using the *in situ* optical Schwarzschild microscope that directly images the surface of the sample and its modification in real time [12]. Electronic gating during the profiling experiments was set to 50%. The resulting depth profiles are illustrated in Fig.6. We determine the time T at which the Mo film is eroded away as a moment at which the Si and Mo (main isotopes 28 and 98 atomic mass units respectively) signals cross. With this fixed, the Mo film deposited for 60 s was eroded in 72 s, the one deposited for 90 s was eroded in 109 s, and the one deposited for 120 s was eroded in 144 s. Using Eq.(2), three thicknesses 7.5 nm (60 s deposition), 11.4 nm (90 s deposition) and 15.1 nm (120 s deposition) were calculated with $j = 17.6 \pm 1.8$ $\mu A/cm^2$; M=95.95 a.m.u.=95.95×1.7×10^{-24} g; ρ=10.28 g/cm^3; e=1.6×10^{-19} C; Y=6.02. Y=6.02 was obtained using SRIM/TRIM [13], a Monte-Carlo code, in the full cascade mode on the ensemble of 10^5 Ar^+ ions with their

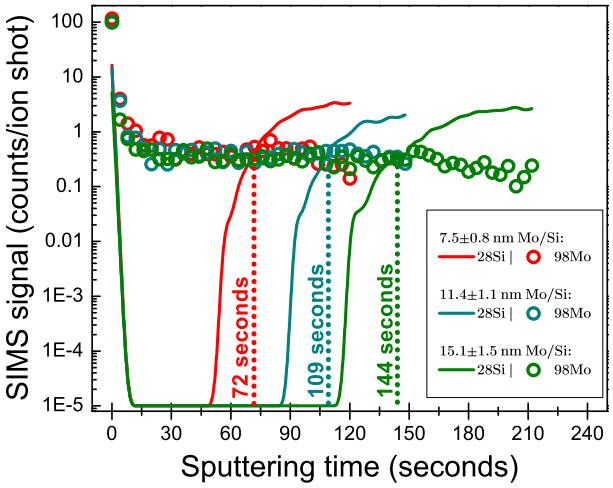

FIG. 6: Depth profiles for Mo films on Si witness coupons

energy set to 5 keV and the irradiation angle set to 60°.

We stress that (1) the apparent spike for the Si signal is due to the presence of the C-O molecule on the surface (no isotopic pattern for Si was observed in a full mass spectrum recorded for the pristine surface, sputtering time=0 s) and (2) the apparent spike for the Mo signal is due to slight metal surface oxidation that always leads to orders of magnitude higher secondary ion signals in SIMS (secondary ion formation probability is higher in metal-oxides compared to clean metals) [14].

The thickness of 7.5 nm explains why the standard Mo/YAG:Ce screen is semitransparent in the visible range (Fig.2), and thus why we observe the combination of green and red photons when imaging electron emission with the YAG:Ce screen (Fig.3). The determined 7.5 nm thickness of the standard Mo coating, being in excellent agreement with electron range calculations, straightforwardly explains why deposition time of 60 s is optimal for imaging with the YAG:Ce phosphor screen at applied voltages of up to 1.1 kV.

Photon sensitivity

Taking it a step forward, let us estimate photon sensitivity of the system. The first step here would be to calculate the electron to 550 nm photon conversion as

$$C_{e\to ph} = T_e^{vac/Mo} \cdot T_e^{Mo} \cdot C_{YAG}, \quad (3)$$

where $T_e^{vac/Mo}$ is the transmission coefficient of electrons through the interface between vacuum and the Mo film (1 minus reflection), T_e^{Mo} is the transmission coefficient of electrons through the Mo film, C_{YAG} is electron-to-photon conversion of all the electrons that penetrate through the Mo film and get embedded in the YAG:Ce screen. $T_e^{vac/Mo}$ is only dependent on Z and is approximately equal to 0.7 [10]. T_e^{Mo} is equal to 0.1 at a Mo thickness close to practical electron range (6.5 nm at 1 keV). We consider C_{YAG}=0.01 [15].

Assuming that 1 keV electrons provide a relatively uniform distribution of a current of 100 μA over an area of 2.2 mm in radius (Fig.1) captured by the Canon 6D on the 500 by 500 pixels sensor area and using the resulting $C_{e\to ph} = 7\times10^{-4}$, we obtain that the signal per pixel is $\sim10^6$ photons/s with a Poisson noise of $\sim10^3$ and a S/N ratio $\approx10^3$. If the current (emission is still considered uniform) is reduced to 100 nA and further to 1 nA (the limit for the Keithley), then the signal per pixel reduces to $\sim10^3$ (S/N$\approx$30) and 10 (S/N$\approx$3) photons/s, respectively. Since the read noise level at ISO=1,000 (used in experiments) in the Canon 6D is between 1 to 5 electrons, such a low electron emission should be still observable by the camera at 1 keV. This would be worst case scenario. In fact, we typically see that emission starts with isolated small features, meaning that even though the current is reduced by many orders of magnitude the local pixel photon density on the sensor can remain very high.

The main factor here is not the current or current density providing the Canon sensor with enough photons per pixel, but the electron energy that should remain higher than 700 eV in order to keep the practical electron range no less than 5 nm. In this sense, Mo/YAG:Ce anode screens with different Mo thicknesses can be combined (up to 3 on the frame holder shown on the schematic diagram in Fig.1) and/or a larger inter-electrode gap used to enable higher electron kinetic energy at the same electric field in order to detect small signals.

At 100 μA and 1 keV and ISO=1,000, we can calculate the photographic equivalent of the light produced on the Mo/YAG:Ce screen, namely, $\sim10^6$ photons per pixel per second corresponds to $\sim10^{16}$ photons per second per m^2. At the wavelength of 550 nm, this is about 1/2 lux or 1 EV. This means that imaging with Mo/YAG:Ce anode screen at 100 μA and 1 keV is equivalent to photographing the full moon on a clear night. At lower currents, it becomes equivalent to taking images of a moonless clear sky with stars.

We note here that the best practice to take pictures in the described arrangement is as follows. The ISO has to be 1,000-3,000, because it drastically reduces pattern/banding noise and electronic noise, and allows better discrimination of small lighting features above the background when collecting for many seconds. Secondly, top level cameras preserve the highest dynamic range above 10 photographic stops, with the dynamic range measured in photographic stops being calculated as $log_2 \frac{fullwellcapacity[electrons]}{totalnoise[electrons]}$. This means that high dynamic range and low noise at ISO of a few thousand enable simultaneous detection of lighting features of exceptionally different brightnesses, from $\sim$10 to $\sim10^5$ photons per pixel. This is an extremely useful capability when one wants to collect images through the entire I-V curve acquisition process, from tens of nA to hundreds of μA.

Vacuum system

In Fig.7, the vacuum diagram of the imager is presented. Evacuation process of the vacuum cham-

ber/vessel is three-fold. The first pumping stage is an oil-free diaphragm pump (ultimate pressure 1.5 Torr). Second stage pumping uses a turbo-molecular pump: the pumping speed for N_2 is 67 l/s, the compression ratio for N_2 and Ar is 10^{11}, the compression ratio for H_2 is 10^5, and the typical ultimate pressure with no high temperature baking is 2×10^{-8} Torr at the backing pressure of 1.5 Torr. The third stage is an ion pump (pumping speed for N_2 is 30 l/s) that is turned on at 5×10^{-6} Torr which significantly improves the pumping speed toward 2×10^{-8} Torr.

To quickly (in about 24 hours) achieve the nominal working pressure of $\approx3\times10^{-9}$ Torr, which is satisfactory enough to perform measurements, the following procedure is established. The vacuum system does not have any single Viton or rubber O-ring connections. All vacuum components such as mechanical holders and screws are ultrasonically cleaned. Step one is to clean in a mixture of distilled water and an acid based detergent performed for about 30 minutes. Step two is to clean in a 50/50 mixture of ethanol and acetone performed for another 30 minutes. All parts are dried using dry nitrogen before installation. All parts undergo a high temperature drying during the first bake out of the system. The routine bake out procedure is as follows. The system is heated to up to 140-145 °C when a pressure of 8×10^{-8} Torr or lower is achieved through the described three-fold procedure. The choice of the bake out temperature is limited by the Pfeiffer full range pirani/cold cathode gauge in use (recommended baking temperature must not exceed 150 °C with magnet detached). The chamber is kept at 140-145 °C for about 12 hours. The measure of a successful baking procedure is if the pressure (with gauge disconnected, calculated via the tabulated "ion current versus pressure" curve provided for the ion pump by the manufacturer) returns to 8×10^{-8} Torr or better at 140-145 °C. After that, the heating is turned off and the chamber naturally cools downs for another 12 hours and reaches the targeted $\approx3\times10^{-9}$ Torr. This procedure is fully automated. The final step is to close an isolation gate valve (the one atop the turbo pump symbol in Fig.7) and turn off the diaphragm and turbo pumps and wait until the pressure stabilizes at $\approx 3\times10^{-9}$ Torr with only the ion pump on. Mechanical vibration free pumping is necessary because field emission systems are sensitive to vibrations resulting in cathode-anode gap fluctuations producing noisy current readings. An SRS residual gas analyzer monitors gas composition in the system and checks for any virtual or actual leaks.

I-V curve measurement and imaging algorithm

The entire data acquisition process is automated using the LabVIEW programming environment. The Keithley 2410 simultaneously acts as a voltage source (active mode: control signal in/feedback voltage reading out) and a pico- to micro-ammeter (passive mode: current reading out). The vacuum reading is taken directly from a Pfeiffer controller connected to the full range pirani/cold cathode gauge. Ion pump current/pressure is acquired using a DAQ 6004 by National Instruments. Electron emission images are taken by the Canon 6D equipped with a 50 mm lens and close-up lenses and extensions; the standard work distance is set at 6 cm.

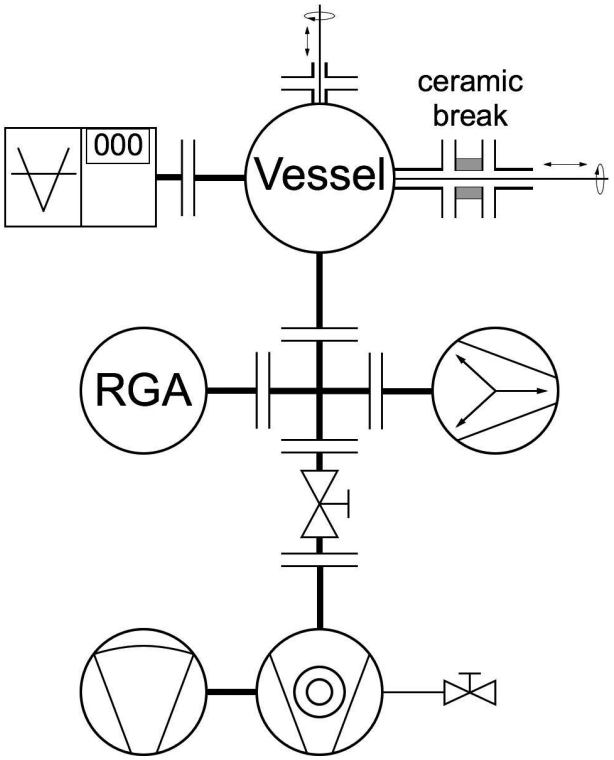

FIG. 7: Vacuum diagram of the imager

Fig.8 illustrates the algorithm to measure current as voltage is swept. After the voltage is increased/decreased and before the current measurement starts, there is a 1 second delay (typically dt_1=1 s, but can be varied down to 0 s) introduced to allow time for the electrometer internal circuit to settle. After the dt_1 delay, the current is sampled n times with a sampling rate $1/dt_2$. Typically n=20 and dt_2=300 ms, but both values can be varied. The current, voltage, and pressure are sampled and processed to obtain the mean value, the standard deviation and the total measurement error. All are calculated online using well-known statistics formulas

$$\bar{x} = \frac{1}{n}\sum_{i=1}^{n} x_i, \quad (4)$$

$$s = \sqrt{\frac{1}{n-1}\sum_{i=1}^{n}(x_i - \bar{x})^2}, \quad (5)$$

$$\Delta x = t_{p,n}\cdot\frac{s}{\sqrt{n}} + \theta, \quad (6)$$

here $t_{p,n}$=2.09 is the Student's t-distribution coefficient for a confidence interval of 95%, n=20 is the number of

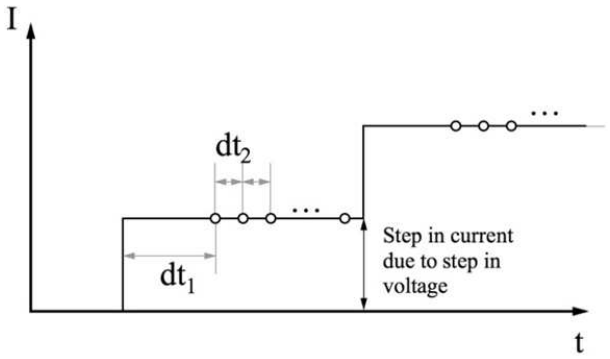

FIG. 8: Schematic diagram of current measurement algorithm

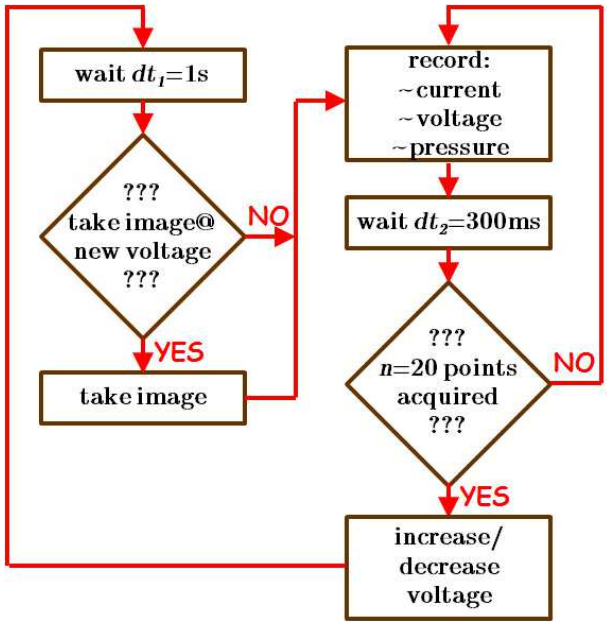

FIG. 9: Block diagram of the LabVIEW software for fully automatic data and image acquisition

measurements at a given voltage, θ=50 pA and 10 μV are the ultimate accuracies of the Keithley 2410 electrometer for current and voltage, respectively. All data, raw and processed, are recorded and stored into files.

The software is designed such that I-V curve measurement and collection of images using Mo/YAG:Ce or ITO/BASG anode screens are synced within a specified run, with the voltage ramped up and down. The entire block diagram is shown in Fig.9. The LabVIEW program allows specification of a voltage step to repeatedly acquire images with the Canon 6D as the voltage is swept up or down. One can specify images to be taken every 20, 50, 100 V, etc. while the voltage is being ramped. The voltage step size can be between 1 V and 1 kV.

Conclusions

We presented a design and detailed description of an apparatus for direct imaging of the electron field emission site distribution on cathodes surfaces. We implemented a projection approach to the imaging problem, making use of anode screens in the standard parallel plate configuration. Detailed characterization and performance metrics of the imaging Mo/YAG:Ce anode screen are given, and recommendations for metal coating procedures are presented based on our experience. In particular, we have calculated electron to photon conversion efficiency as well as measured the response and sensitivity of the optical system to the emitted current. We also estimated that the lateral spatial resolution of the imager is on the order of 1 μm. As a part of the imaging apparatus, the fully automated vacuum control/monitor and data acquisition software was described.

The commissioned electron emission projection imager, in combination with microscopy and spectroscopic methods, may unveil electron emission induced processes on the micron and submicron scale.

Acknowledgment

Euclid was supported by the Office of Nuclear Physics of DOE through a Small Business Innovative Research grant # DE-SC 0013145. We also thank

Alexander Zinovev of Materials Science Division at ANL for providing the access to SARISA, a mass spectrometer. Use of SARISA was supported by the U.S. Department of Energy, Office of Science, Materials Sciences and Engineering Division.

Kiran Kovi and Anirudha Sumant of the Center of Nanoscale Materials at ANL for providing us with the CNT sample. Use of the Center for Nanoscale Materials, an Office of Science user facility, was supported by the U.S. Department of Energy, Office of Science, Office of Basic Energy Sciences, under Contract No. DE-AC02-06CH11357.

Jiaqi Qiu and Richard Konecny of Euclid TechLabs for their kind help with some of hardware manufacture.

SEM measurements were conducted in the Electron Microscopy Center of the Center for Nanoscale Materials at Argonne National Laboratory. Use of the Center for Nanoscale Materials, an Office of Science user facility, was supported by the U.S. Department of Energy, Office of Science, Office of Basic Energy Sciences, under Contract No. DE-AC02-06CH11357.

† Electronic address: sergey.v.baryshev@gmail.com

[1] D. Lysenkov and G. Müller, Int. J. Nanotechnol. **2**, 239 (2005).

[2] D. Lysenkov, Optimization of nanostructures for field emission cathodes, Ph.D. thesis (2006).

[3] A. V. Karabutov, V. D. Frolov, S. M. Pimenov, and V. I. Konov, Diamond Relat. Mater. **8**, 763 (1999).

[4] S. T. Purcell, P. Vincent, C. Journet, and V. T. Binh, Phys. Rev. Lett. **88**, 105502 (2002).

[5] M. Sveningsson, M. Jönsson, O. A. Nerushev, F. Rohmund, and E. E. B. Campbell, Appl. Phys. Lett. **81**, 1095 (2002).

[6] J. Wei, H. Zhu, D. Wu, and B. Wei, Appl. Phys. Lett. **84**, 4869 (2004).

[7] D. Mann, Y. K. Kato, A. Kinkhabwala, E. Pop, J. Cao, X. Wang, L. Zhang, Q. Wang, J. Guo, and H. Dai, Nature Nanotechnol. **2**, 33 (2007).
[8] M. Cahay, P. T. Murray, T. C. Back, S. Fairchild, J. Boeckl, J. Bulmer, K. K. K. Koziol, G. Gruen, M. Sparkes, F. Orozco, and W. O'Neill, Appl. Phys. Lett. **105**, 173107 (2014).
[9] K. Kanaya and S. Okayama, J. Phys. D **5**, 43 (1972).
[10] J. I. Goldstein, D. E. Newbury, P. Echlin, D. C. Joy, C. Fiori, and E. Lifshin, Scanning electron microscopy and X-ray microanalysis: a text for biologists, materials scientists, and geologists (Plenum Press, New York, 1981).
[11] S. V. Baryshev, N. G. Becker, A. V. Zinovev, C. E. Tripa, and I. V. Veryovkin, Rapid Commun. Mass Spectrom. **27**, 2828 (2013).
[12] I. V. Veryovkin, C. Emil Tripa, and M. J. Pellin, Phys. Procedia **1**, 379 (2008).
[13] J. F. Ziegler, M. D. Ziegler, and J. P. Biersack, Nucl. Instrum. Methods Phys. Res. B **268**, 1818 (2010).
[14] A. Benninghoven and A. Mueller, Phys. Lett. A **40**, 169 (1972).
[15] P. Schauer and R. Autrata, Performance of YAG:Ce single crystal screens for TEM, Proc. 14th International Congress on Electron Microscopy (1998).